Pump-probe spectroscopy using quantum light with two-photon coincidence detection

F. Schlawin, K. E. Dorfman, and S. Mukamel

Phys. Rev. A **93**, 023807 — Published 3 February 2016

DOI: 10.1103/PhysRevA.93.023807

Pump-probe spectroscopy using quantum light with two-photon coincidence detection

F. Schlawin,[1,*] K. E. Dorfman,[2] and S. Mukamel[2]

[1]*Physikalisches Institut, Albert-Ludwigs-Universität Freiburg, Hermann-Herder-Straße 3, 79104 Freiburg, Germany*
[2]*Department of Chemistry, University of California, Irvine, California 92697, USA*

We propose a pump-probe signal, whereby the sample is excited by a classical pulse, and - after a variable time delay - probed by a photon from an entangled pair, which is finally detected in coincidence with its twin. This setup offers an improved time and frequency resolution compared to a classical pump-probe signal, and can be used to enhance or suppress selected resonances.

PACS numbers: 42.62.Fi, 78.47.jh, 42.65.Lm

I. INTRODUCTION

Quantum light is gaining attention as a possible tool in (nonlinear) spectroscopy, where its nonclassical quantum fluctuations [1], its linear scaling behavior [2–4] or its nonclassical bandwidth properties [5–8] may be exploited to enhance frequency or time resolution beyond classically achievable limits. Here, we focus on the latter case, where it has been shown that the nonclassical bandwidth properties of entangled photons allow the control of two-exciton states in molecular aggregates [9, 10] or of vibrational states in molecules [11, 12]. The two-photon wavefunction further offers new control parameters for the manipulation of optical signals [8].

Entangled photons have already been employed successfully in linear "biphoton spectroscopy", whereby they are detected in coincidence [13–16]. This technique has been shown to suppress background in noisy samples. In contrast to direct two-photon absorption measurements [4], only one of the two photons interacts with the sample. The idle photon serves as a reference for the arrival of its twin, making use of the strong correlations in the arrival time of the two photons, and the other photon is detected in a monochromator, exploiting the spectral correlations of the two photons [5, 6]. As shown in Ref. [17], the combined time-frequency entanglement of the photons may be put to use in nonlinear spectroscopy by enhancing the resolution, and selecting specific pathways in stimulated Raman spectroscopy. This Article extends these ideas to simulate a pump-probe measurement combined with two-photon counting (TPC) detection. Utilizing a simple toy model, we explore how the two-photon counting setup may be used to filter the signal, and enhance or suppress selected features.

In section II, we introduce the setup, and derive formal expressions for the TPC signal, as well as the classical pump-probe signal. This will enable us to simulate the nonlinear optical response of the two state jump (TSJ) model in section III.

* frank.schlawin@physik.uni-freiburg.de

II. THE SETUP AND SIGNAL

We consider a system consisting of the light field, and a material system, which is surrounded by a dissipative environment. Hence, the total Hamiltonian is given by

$$H_{\text{total}} = H_{\text{system}} + H_{\text{bath}} + H_{\text{BS}} + H_{\text{field}} + H_{\text{int}}. \tag{1}$$

The five terms represent the system, the bath, their interaction, the field, and the field-matter interaction Hamiltonian in the dipole approximation, respectively. Here, we work in the interaction picture with respect to $H_{\text{system}}+H_{\text{bath}}+H_{\text{BS}}+H_{\text{field}}$, such that the interaction Hamiltonian reads

$$H_{\text{int}}(t) = E(t)V^\dagger(t) + E^\dagger(t)V(t), \tag{2}$$

where $E(t)$ ($E^\dagger(t)$) denotes the positive-(negative-)frequency component of the sum of all the fields considered, and $V(t)$ ($V^\dagger(t)$) the sample de-excitation (excitation) operator. The quantum field operator is given by

$$E(t) = \int \frac{d\omega}{\sqrt{2\pi}} e^{-i\omega t} a(\omega), \tag{3}$$

with $a(\omega)$ being the photon annihilation operator at frequency ω, which satisfies the bosonic commutation relation $[a(\omega), a^\dagger(\omega')] = \delta(\omega-\omega')$. For clarity in our definition of the electromagnetic field (3), we have omitted the field normalization, which has been absorbed into the (de-)excitation operators.

We consider the setup depicted in Fig. 1a): A pair of entangled photons, that has been created, e.g., by parametric down-conversion in a birefringent crystal, hits a beam splitter. One photon is sent through the sample, which has previously been excited by a classical ultrafast laser pulse, and then detected. The other photon serves as a reference (ancilla), and is detected in coincidence. To provide a new window for the signal, we exploit the quantum correlations shared between the two photons.

The two-photon counting signal is spectrally dispersed, and our signal is given by the change to this two-photon counting rate [18, 19]

$$\langle E_2^\dagger(\omega_r) E_1^\dagger(\omega) E_1(\omega) E_2(\omega_r)\rangle \tag{4}$$

due to the interaction with the sample. Here, ω/ω_r denotes the detected frequency of the respective beam, and the brackets $\langle\cdots\rangle$ represent the expectation value with respect to the

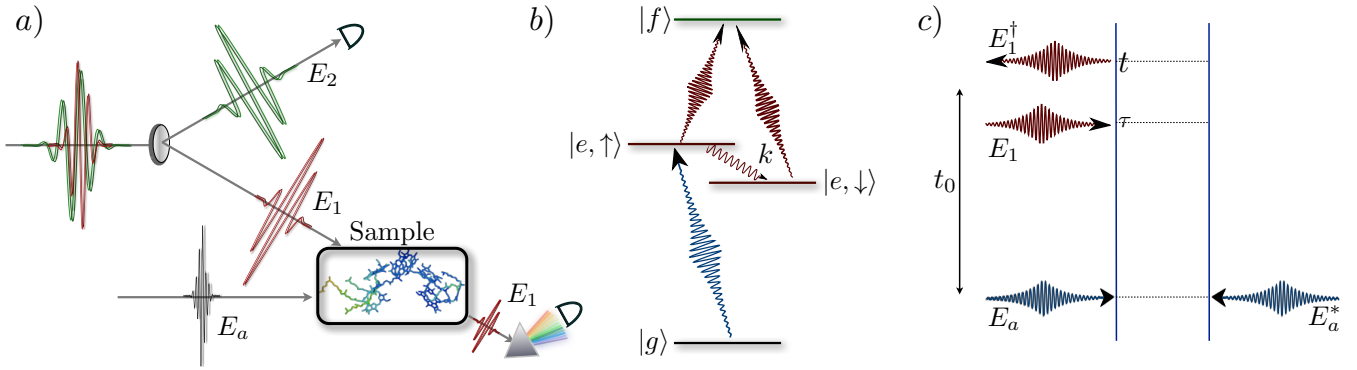

FIG. 1. (Color online) a) The proposed TPC setup: the entangled photon pair in beams E_1 and E_2 are split on a beam splitter. A classical, actinic, ultrafast pulse E_a excites the sample, and E_1 is employed as a probe in a pump-probe measurement, while E_2 is spectrally dispersed, and detected in coincidence. b) The level scheme for the two-state jump (TSJ) model considered in this work. The $g-e$ transition is driven by the actinic pulse (blue arrow). It is far off-resonant from the spectral range of the entangled photon wavepacket (red arrows), which only couples to the $e-f$ transition. c) Diagram representing the pump-probe measurement.

transmitted fields. As shown in appendix A, the change is given by

$$S_{\mathrm{TPC}}(\Gamma) = \frac{2}{\hbar}\Im\int dt\, e^{i\omega(t-t_0)}\mathrm{tr}\left\{E_2^\dagger(\omega_r)E_1^\dagger(\omega)V(t)E_2(\omega_r)\varrho(t)\right\}, \tag{5}$$

where Γ denotes the set of control parameters of the fields (to be specified later). $\varrho(t)$ represents the density matrix of the combined matter + field system, and is given by the Dyson series

$$\varrho(t) = \mathcal{T}\exp\left[-\frac{i}{\hbar}\int_{t_0}^{t} d\tau H_{\mathrm{int},-}(\tau)\right]\varrho_{\mathrm{initial}}, \tag{6}$$

and the initial density matrix

$$\varrho_{\mathrm{initial}} = |g\rangle\langle g|\otimes\varrho_{\mathrm{field}}, \tag{7}$$

where ϱ_{field} is specified in appendix B. Here, $\mathcal{T}$ is the time-ordering operator, and $H_{\mathrm{int},-}$ the Liouville Superoperator, defined by $H_{\mathrm{int},-}X = H_{\mathrm{int}}X - XH_{\mathrm{int}}$. The trace in Eq. (5) is taken with respect to the full (molecule + field) Hilbert space, given by H_{tot}.

To obtain the pump-probe signal in a three-level system, we expand the exponential in Eq. (6) to third order. The first two interactions are with the classical pump pulse, which is taken to be impulsive, $E_a(t) = E_a\delta(t)$, and the third is with the probe. Assuming E_1 to be far off-resonant from the $e-g$ transition, we obtain only the single diagram shown in Fig. 1c), which reads

$$S_{\mathrm{TPC}}(\Gamma) = -\frac{2}{\hbar}\Im\left(-\frac{i}{\hbar}\right)^3|E_a|^2\int_0^\infty dt\, e^{i\omega(t-t_0)}\int_0^t d\tau\, F(t-\tau,\tau) \times\langle E_2^\dagger(\omega_r)E_1^\dagger(\omega)E_1(\tau)E_2(\omega_r)\rangle. \tag{8}$$

We have defined the matter correlation function,

$$F(t-\tau,\tau) = \langle|\mu_{ge}|^2|\mu_{ef}|^2G_{fe}(t-\tau)G_{ee}(\tau)\rangle_{\mathrm{env}}, \tag{9}$$

where μ_{ge} and μ_{ef} denote the dipole moments connecting ground state with the single exciton manifold, as well as single with two-exciton manifold, respectively. $\langle\cdots\rangle_{\mathrm{env}}$ denotes the average with respect to environmental degrees of freedom, obtained from tracing out the bath. Decomposing the field operator spectrally,

$$E_1(\tau) = \int\frac{d\omega_b}{\sqrt{2\pi}}\, e^{-i\omega_b(\tau-t_0)}E_1(\omega), \tag{10}$$

we can carry out the time integrations in Eq. (8) to obtain

$$S_{\mathrm{TPC}}(\omega,\omega_r;t_0) = \frac{2}{\hbar^4}|E_a|^2\Re\int\frac{d\omega_b}{\sqrt{2\pi}}\,\tilde{F}(\omega_b,\omega;t_0) \times\langle E_2^\dagger(\omega_r)E_1^\dagger(\omega)E_1(\omega_b)E_2(\omega_r)\rangle, \tag{11}$$

with

$$\tilde{F}(\omega_b,\omega;t_0) \equiv \int_0^\infty dt\int_0^t d\tau\, F(t-\tau,\tau)\, e^{i\omega(t-t_0)}e^{-i\omega_b(\tau-t_0)}. \tag{12}$$

Here, we also specified the control parameters we employ in this Article: the two frequencies ω and ω_r, at which the two photons are detected, and the time delay t_0.

For comparison, we present the classical pump-probe signal (*i.e.* change in transmission of a classical probe pulse), which will serve as a reference for the two-photon counting signal. The change in transmission is obtained by measuring the intensity of a classical probe pulse

$$\langle E_{pr}^\dagger(\omega)E_{pr}(\omega)\rangle. \tag{13}$$

Its change induced by the interaction with the sample is given by [20]

$$S_{\mathrm{PP}}(t_0,\omega) = \frac{2}{\hbar}\Im E_{pr}^*(\omega)\langle V(\omega)\rangle, \tag{14}$$

where we have already replaced the field operator by the classical field envelope E_{pr}, and taken it out of the expectation

value. By comparison with Eq. (8), we can see that we may obtain the classical pump-probe signal by replacing the field correlation function $\langle E_2^\dagger(\omega_r)E_1^\dagger(\omega)E_1(\omega_b)E_2(\omega_r)\rangle$ with the classical field envelope of the probe pulse. Hence, we arrive at

$$S_{\rm PP}(t_0,\omega) = \frac{2}{\hbar}\Im\left(-\frac{i}{\hbar}\right)^3 |E_a|^2 \int_0^\infty dt\, e^{i\omega t}\int_0^t d\tau \times E_{pr}^*(\omega)E_{pr}(\tau)F(t-\tau,\tau), \tag{15}$$

which can be recast in the frequency domain

$$S_{\rm PP}(t_0,\omega) = \frac{2}{\hbar^4}|E_a|^2\Re\int\frac{d\omega_b}{\sqrt{2\pi}}\, E_{pr}^*(\omega)E_{pr}(\omega_b)\tilde{F}(\omega_b,\omega;t_0). \tag{16}$$

Comparison of Eqs. (11) and (16) reveals that the classical pump-probe signal has precisely the same matter information as the TPC signal. However, as we will show in the following - the four-point correlation function in Eq. (8) offers a novel window for filtering the signal, which can enhance desired features.

III. SIMULATIONS OF CLASSICAL AND QUANTUM PUMP-PROBE SIGNALS BY THE STOCHASTIC LIOUVILLE EQUATIONS

We do not treat the bath explicitly, but rather average our final expressions over bath realizations to obtain an effective master equation for the system evolution. This level of theory is known as the stochastic Liouville equation [21]. Here, we employ the two-state jump (TSJ) model: A ground state g is dipole-coupled to an electronic excited state e, which is connected to two spin states $\uparrow$ and $\downarrow$ undergoing relaxation [22]. We additionally consider a two-exciton state f, which is dipole-coupled to both $|e,\uparrow\rangle$ and $|e,\downarrow\rangle$ [see Fig. 1b)]. The electronic states are damped by a dephasing rate γ. We only consider the low-temperature limit of this model, where only the decay process from $\uparrow$ to $\downarrow$ is allowed [23]. The decay process is entirely incoherent, such that the description may be restricted to the two spin populations $|\uparrow\rangle\langle\uparrow| \hat{=}(1,0)^T$ and $|\downarrow\rangle\langle\downarrow| \hat{=}(0,1)^T$. The propagator in the e-population is then given by [23]

$$\mathcal{G}_{ee}(t) = \Theta(t)\begin{pmatrix} e^{-kt} & 0 \\ 1-e^{-kt} & 1\end{pmatrix}, \tag{17}$$

where k denotes the decay rate of the spin relaxation. The coherence between f and e reads

$$\mathcal{G}_{fe}(t) = \Theta(t)\begin{pmatrix} e^{-(k+i\omega_-)t} & 0 \\ \frac{k}{k+2i\delta}\left[e^{-i\omega_+t}-e^{-(k+i\omega_-)t}\right] & e^{-i\omega_+t}\end{pmatrix}, \tag{18}$$

with δ the energy difference between the two spin states, and $\omega_\pm = \omega_{fe}\pm\delta$. Note that, since we monitor the $f-e$ transition, the detected frequency will increase in time, from ω_- to ω_+. The field correlation function (9) is then given by

$$\begin{aligned} F(t_2,t_1) &= \langle\langle Id||\mu_{ge}|^2|\mu_{ef}|^2 G_{fe}(t_2)G_{ee}(t_1)|\uparrow\rangle\rangle \\ &= |\mu_{ge}|^2|\mu_{ef}|^2 e^{-\gamma(t_1+2t_2)} \\ &\times\left(e^{-i\omega_+t_2} + \frac{2i\delta}{k+2i\delta}e^{-kt_1}\left[e^{-(k+i\omega_-)t_2}-e^{-i\omega_+t_2}\right]\right). \end{aligned} \tag{19}$$

Its counterpart in frequency domain is then given by

$$\begin{aligned} \tilde{F}(\omega_b,\omega;t_0) = |\mu_{ge}|^2|\mu_{ef}|^2\Bigg(&\frac{e^{-i(\omega-\omega_b)t_0}}{\omega_b-\omega_+-i\gamma}\left[\frac{1}{\omega-\omega_b+2i\gamma}-\frac{1}{\omega-\omega_++i\gamma}\right] \\ &+\frac{2i\delta}{k+2i\delta}\frac{e^{-i(\omega-\omega_b)t_0}}{\omega_b-\omega_--i\gamma}\left[\frac{1}{\omega-\omega_b+i(k+2\gamma)}-\frac{1}{\omega-\omega_-+i(k+\gamma)}\right] \\ &-\frac{2i\delta}{k+2i\delta}\frac{e^{-i(\omega-\omega_b)t_0}}{\omega_b-\omega_+-i(k+\gamma)}\left[\frac{1}{\omega-\omega_b+i(k+2\gamma)}-\frac{1}{\omega-\omega_++i\gamma}\right]\Bigg). \end{aligned} \tag{20}$$

The field correlation function in Eq. (11), which will be used below, is derived in appendix B.

In the following, we use these results to first simulate the classical pump-probe signal, and then the two-photon counting signal with entangled photons. For the former case, we consider a classical probe pulse in our simulations with a Gaussian envelope,

$$E_{pr}(\omega) = \frac{1}{\sqrt{2\pi\sigma^2}}\exp\left[-(\omega-\omega_0)^2/2\sigma^2\right]. \tag{21}$$

We chose the following system parameters: $\omega_{fe} = 11{,}000$ cm^{-1}, $\delta = 200$ cm^{-1}, $k = 120$ cm^{-1}, and $\gamma = 100$ cm^{-1}.

Fig. 2 depicts the classical pump-probe signal vs. the dispersed frequency ω and the time delay t_0, where we have normalized each plot to its maximal peak.

The center frequency ω_0 is fixed at the transition frequency ω_{fe}, and we vary the probe bandwidth. Panel a) shows the signal for $\sigma = 1{,}000$ cm^{-1}. Two peaks at $\omega_{fe}\pm\delta$ correspond to the detected frequency, when the system is either in the upper state (at $\omega_{fe}-\delta$), or in the lower state ($\omega_{fe}+\delta$). Due to the spectrally dispersed detection of the signal, the resonance widths

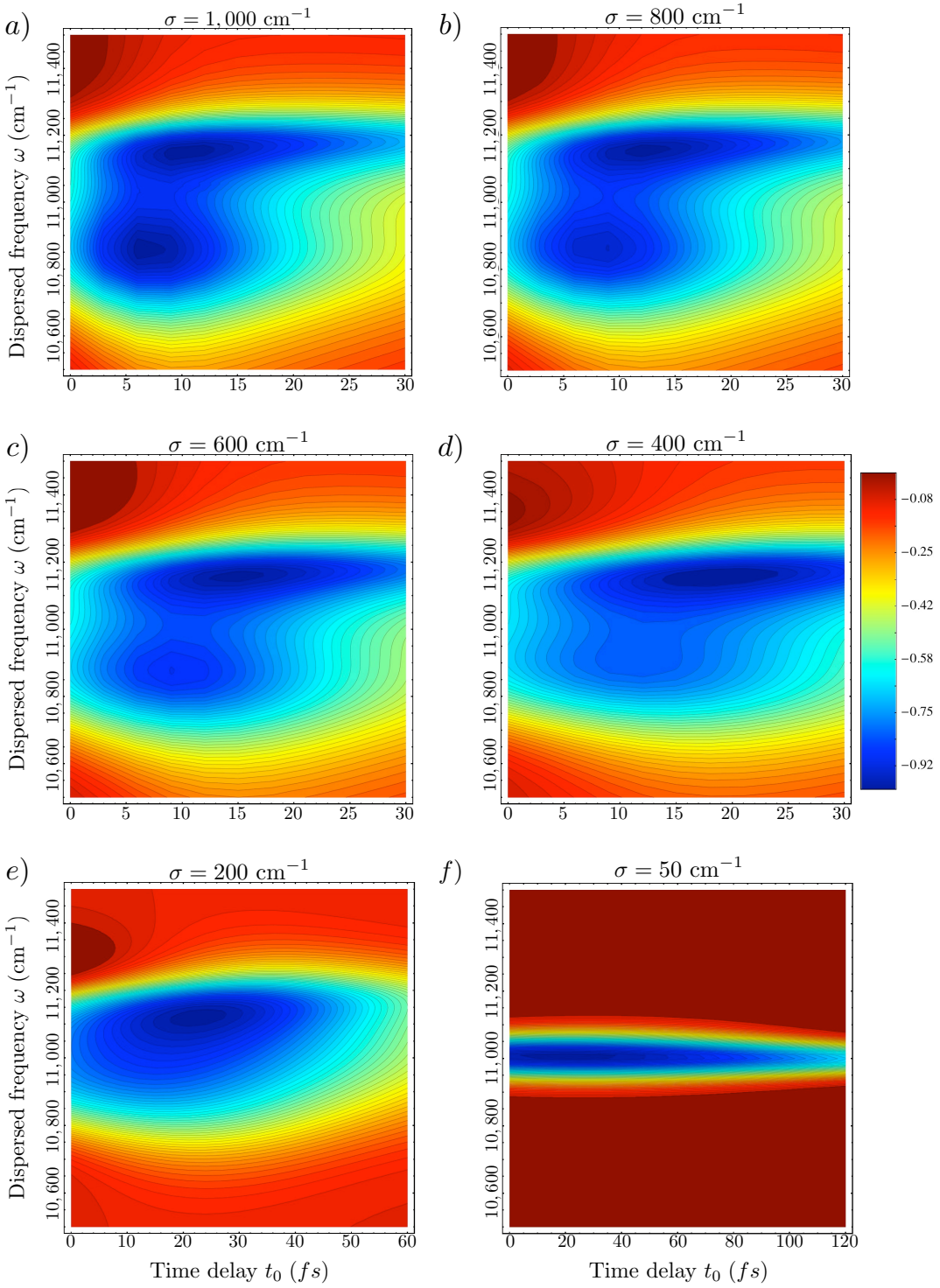

FIG. 2. (Color online) The classical pump-probe signal, Eq. (16), displayed vs. the time delay to the pump pulse t_0 (in fs), and the dispersed frequency ω (in cm^{-1}) with a probe bandwidth of a) $\sigma = 1,000$ cm^{-1} (*i.e.* 5.6 fs), b) 800 cm^{-1}, c) 600 cm^{-1}, d) 400 cm^{-1}, e) 200 cm^{-1}, and f) 50 cm^{-1} (111 fs). The center frequency of the probe beam is fixed at $\omega_0 = 11,000$ cm^{-1}.

are given by the linewidth γ, and not the much broader probe pulse bandwidth σ. For very short time delays t_0, both resonances increase, until the probe pulse has fully passed through the sample. Then the resonance at $10,800$ cm^{-1}, *i.e.* the state $|e,\uparrow\rangle$, starts to decay rapidly, while the resonance at $11,200$ cm^{-1} peaks at longer delay times due to its initial population by the upper state. For longer delays, both resonance decay due to the additional dephasing. With decreasing bandwidth

[panels b) - f)], the temporal resolution decreases as well. This can be seen from the fact that the primary resonance at $\omega_{fe}-\delta$ loses relative intensity, and may no longer be observed for $\sigma \leq 400$ cm^{-1}. Furthermore, the two resonances merge into a single resonance at the unperturbed transition frequency ω_{fe}, since the fast decay process connecting the two resonances may no longer be resolved (motional narrowing) [21].

We now discuss how the frequency correlations between the entangled photons may filter the classical pump-probe signal.

The two-photon counting signal with entangled photons offers several novel control parameters: The dispersed frequency ω of beam 1, the pump frequency ω_p and its bandwidth σ_p loosely correspond to the classical control parameters, *i.e.* the central frequency ω_0 and bandwidth σ. In addition, we may vary the entanglement time T and the detected frequency of the reference beam ω_r.

Fig. 3 shows $S_{\mathrm{TPC}}(\omega, \omega_r; t_0)$ vs. the dispersed frequency ω and the time delay t_0. The pump bandwidth is set to $\sigma_p = 1,000$ cm^{-1} (corresponding to a 5.6 fs pulse) in the top row, and to $2,000$ cm^{-1} in the bottom row. The central frequency of the photon beams is fixed on resonance with the electronic transition, *i.e.* $\omega_p/2 = \omega_{fe}$. In the four panels, we vary the entanglement time T and the reference frequency ω_r. In the left column [panels a) and c)], the reference frequency ω_r is set to $10,400$ cm^{-1}, close to the lower-energy resonance $\omega_{fe}-\delta$. Because of the frequency correlations of the entangled photon pair, this setup enhances the low-energy resonance, and suppresses the high-energetic one. Similarly, in the right column [panels b) and d)], the reference frequency is changed to $11,400$ cm^{-1}, thus enhancing $\omega_{fe}+\delta$, and suppressing the other one.

The remaining new control parameter - the entanglement time T - is varied in the two rows in Fig. 3. The upper row [panels a) and b)] depicts the signal obtained from entangled photons with $T = 90$ fs, and the bottom row [panels c) and d)] with $T = 358$ fs. The longer entanglement time can select a very narrow frequency window from the total signal, and to investigate the relaxation dynamics of this part of the signal separately. In panel d), we identify a build-up of the maximal signal, and its ensuing decay. Panel c) can only resolve the decay of the signal. However, we also observe that - even though we increased the pump bandwidth compared to panels a) and b) - (to $\sigma_p = 2,000$ cm^{-1}) the larger entanglement time results in the loss of time resolution: Even though the maximum in panel d) can be attributed to the intermediate decay $|\uparrow\rangle \rightarrow |\downarrow\rangle$, the signal is widely stretched along the t_0-axis, and the real time constants cannot be read off in this plot.

Fig. 4 depicts slices of panels a) and b) of Fig. 3 for different time delays t_0. For comparison, we show the classical pump-probe with bandwidth $\sigma = 1,000$ cm^{-1} in the left column, and with 100 cm^{-1} in the right column. The TPC signals are normalized with respect to the maximum value of the signal at $t_0 = 3$ fs and $\omega_r = 11,400$ cm^{-1}. The classical signal is normalized to its peak value at zero time delay, and the TPC signals to the signal with $\omega_r = 11,400$ cm^{-1} at zero delay. As discussed before, the panels show that a broadband classical probe pulse (left column) cannot excite specific states, such that the two resonances merge into one band. A narrowband probe (right column), on the other hand, cannot resolve the fast relaxation at all, and only shows the unperturbed resonance at ω_{fe}. TPC spectroscopy, however, can target the relaxation dynamics of the individual states.

IV. CONCLUSIONS

We have shown that TPC spectroscopy with entangled photons provides a novel spectroscopic tool, and demonstrated how it may be used to simplify congested spectra. This feature may be understood by investigating the field correlation functions in Fig. 5b): We depict the $\omega_r - \omega_b$ plot of the entangled photon field correlation function that creates the signal. Clearly, we observe strong positive frequency correlations, and by tuning ω_r, we may select a specific frequency window, from which the signal is created. Conversely, the classical product of field amplitudes in panel a) shows no such correlations, and cannot be used to filter the signal.

Our results add a new angle to the already demonstrated enhanced signal-to-noise ratio of TPC spectroscopy in noisy samples [16].

V. ACKNOWLEDGEMENTS

F. S. thanks the German National Academic Foundation for support. K. E. D. and S. M. gratefully acknowledge the support of the National Science Foundation through Grant No. CHE-1058791, and the Chemical Sciences, Geosciences and Biosciences Division, Office of Basic Energy Sciences, Office of Science, US Department of Energy.

Appendix A: Derivation of TPC signal

To evaluate the change of the two-photon counting signal caused by the interaction with the sample, we start with the full signal,

$$S'_{\mathrm{TPC}}(\Gamma) = \int dt \int dt'\, e^{i\omega(t-t')} \mathrm{tr}\Big\{ E_2^\dagger(\omega_r) E_1^\dagger(t) E_1(t') E_2(\omega_r) \times \mathcal{T} \exp\left[-\frac{i}{\hbar} \int_{-\infty}^{\infty} d\tau H_{\mathrm{int},-}(\tau) \right] \varrho_{\mathrm{initial}} \Big\}, \tag{A1}$$

where, in the second line, we have rewritten the field operators $E_1^\dagger(\omega)E_1(\omega)$ in their time representation. Note that the two interactions at t and t' are not time-ordered, but only the Dyson series of the interaction Hamiltonian. The Dyson series is propagated to infinity, which may seem contradictory at first glance. However, the interaction Hamiltonian can only create a contribution to the measured coincidence rate, if the last interaction predates either t or t'.

Expanding the exponential in the Dyson series to leading order yields

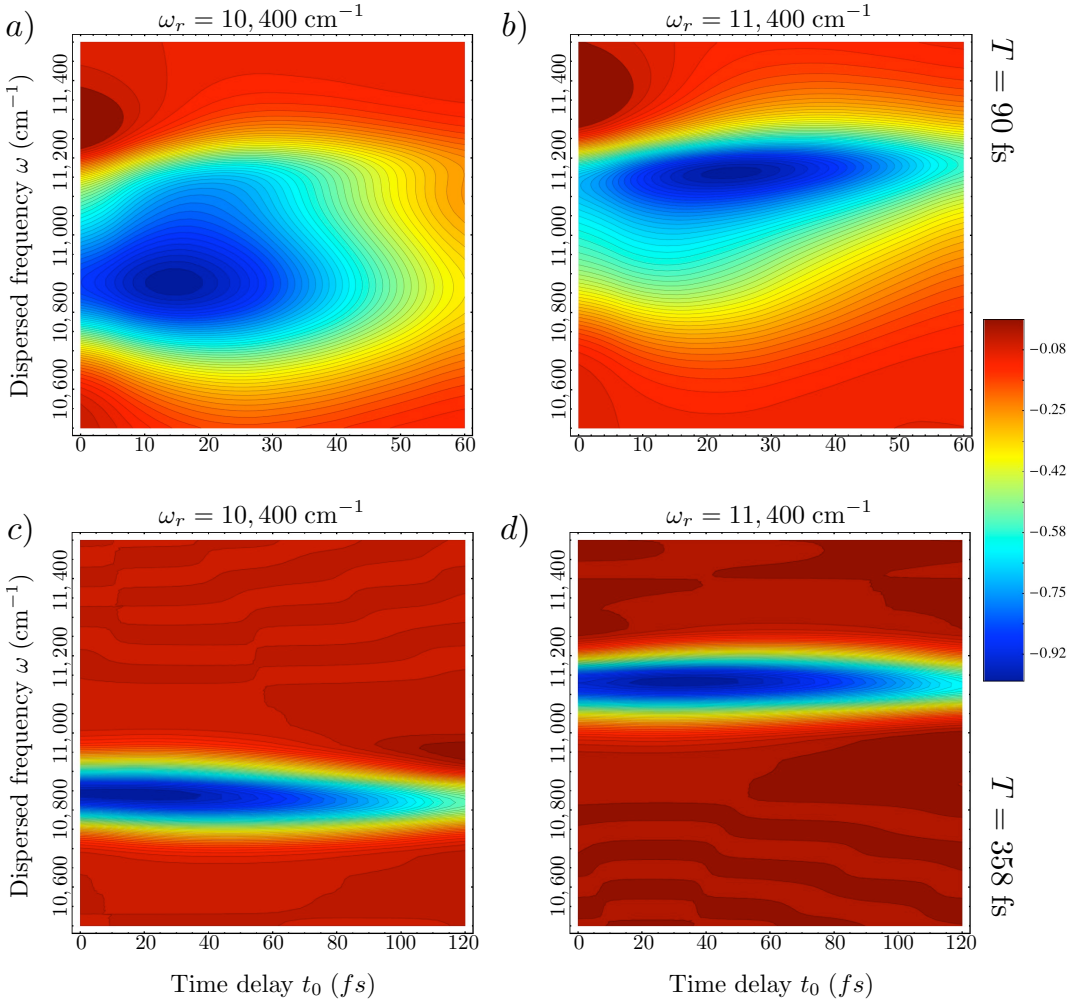

FIG. 3. (Color online) Two-photon counting frequency-dispersed signal of entangled photons $S_{\mathrm{TPC}}(\omega, \omega_r; t_0)$, Eq. (11), with a) $\omega_r = 11,400$ cm^{-1}, $T = 90$ fs, and $\sigma_p = 1,000$ cm^{-1}, b) $\omega_r = 10,400$ cm^{-1}, $T = 90$ fs, and $\sigma_p = 1,000$ cm^{-1}, c) $\omega_r = 11,400$ cm^{-1}, $T = 358$ fs, and $\sigma_p = 2,000$ cm^{-1}, and d) $\omega_r = 10,400$ cm^{-1}, $T = 358$ fs, and $\sigma_p = 2,000$ cm^{-1}. The center frequency of the entangled photons is fixed at $\omega_1 = \omega_2 = 11,000$ cm^{-1}.

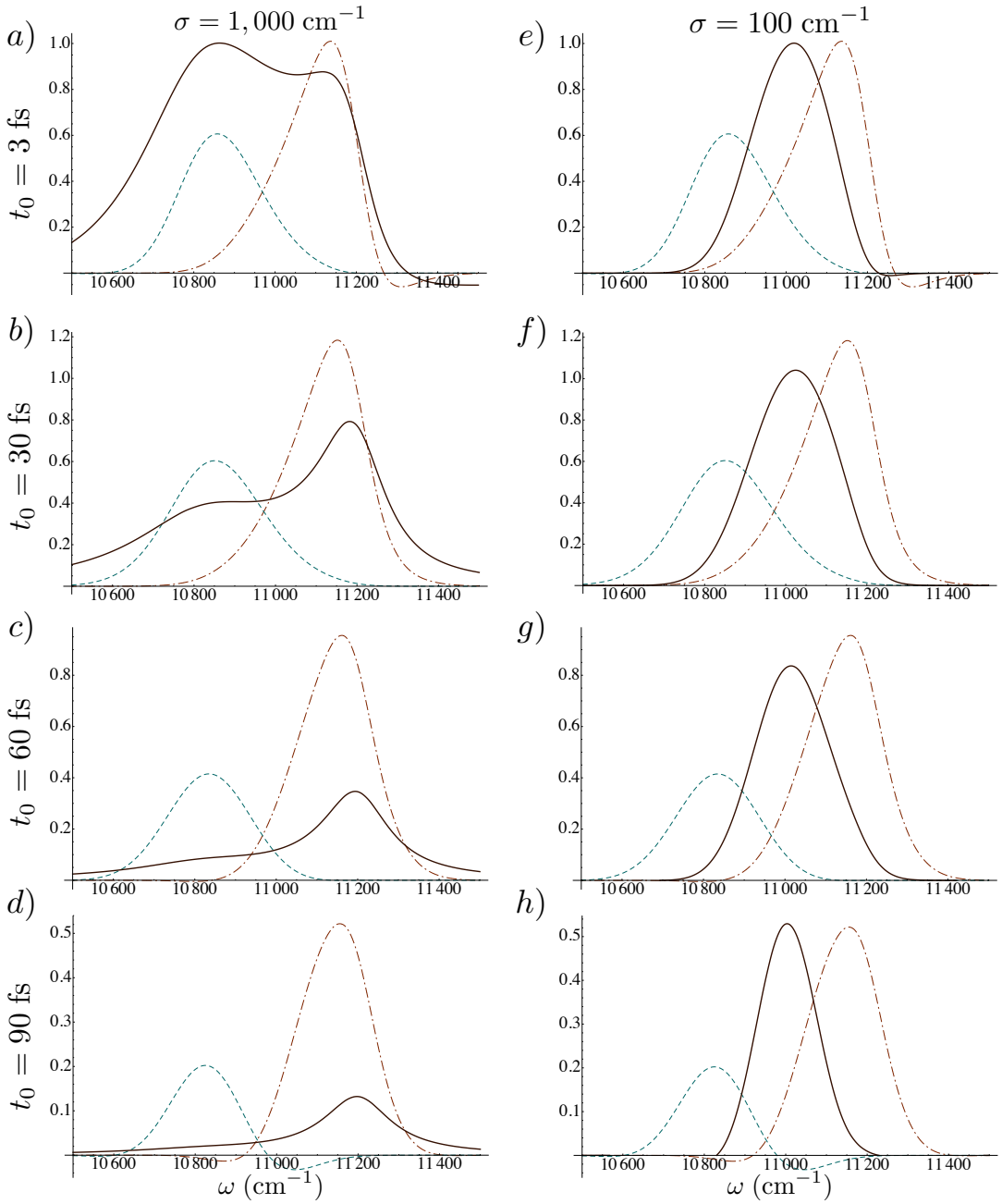

FIG. 4. (Color online) a) TPC signals with $\sigma_p = 2,000\ \mathrm{cm}^{-1}$ and $T = 90$ fs, $\omega_r = 10,400\ \mathrm{cm}^{-1}$ (blue, dashed) and $11,400\ \mathrm{cm}^{-1}$ (red, dot-dashed) as well as the classical pump-probe signal (black, solid) with $\sigma = 1,000\ \mathrm{cm}^{-1}$ are plotted vs. the dispersed frequency ω with a time delay set to $t_0 = 3$ fs. b) Same for $t_0 = 30$ fs, c) 60 fs, d) 90 fs. e)-h) Same as a)-d), but with classical bandwidth $\sigma = 100\ \mathrm{cm}^{-1}$.
The classical signal is normalized, such that its maximum value at $t_0 = 0$ is equal to one. Similarly, the TPC signal are normalized to the maximum value of the signal with $\omega_r = 11,400\ \mathrm{cm}^{-1}$ at $t_0 = 0$.

$$S'_{\mathrm{TPC}}(\Gamma) = \mathrm{tr}\Big\{E_2^\dagger(\omega_r)E_1^\dagger(\omega)E_1(\omega)E_2(\omega_r)\varrho_{\mathrm{initial}}\Big\}$$
$$-\frac{i}{\hbar}\int dt\int dt'\int_{-\infty}^{\infty}d\tau\; e^{i\omega(t-t')}\mathrm{tr}\Big\{E_2^\dagger(\omega_r)E_2(\omega_r)E_1^\dagger(t)E_1(t')\mathcal{T}H_{\mathrm{int},-}(\tau)\exp\left[-\frac{i}{\hbar}\int_{-\infty}^{\tau}d\tau' H_{\mathrm{int},-}(\tau')\right]\varrho_{\mathrm{initial}}\Big\}. \qquad \text{(A2)}$$

The first term in this expansion represents the two-photon counting rate in the absence of any interaction with the sample system, and may therefore be neglected. Our signal - the change of the count rate due to the interaction with the sample - is given by the

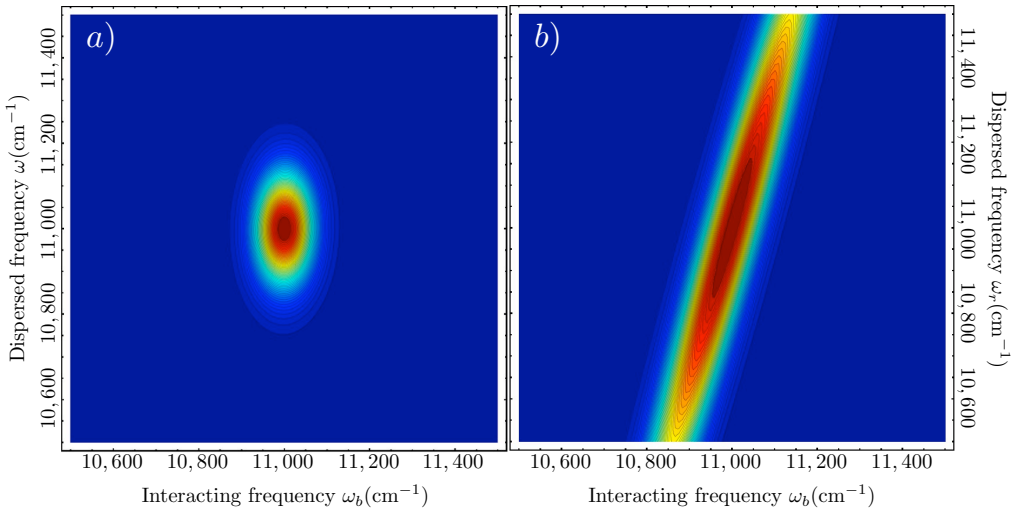

FIG. 5. (Color online) a) Absolute value of the product of uncorrelated classical light envelopes, $E^*_{pr}(\omega)E_{pr}(\omega_b)$, with $\sigma = 100$ cm^{-1}. b) Absolute value of the coherent correlation function, Eq. (B5), of degenerate, entangled photon pairs with $\sigma_p = 400$ cm^{-1}, $T = 900fs$.

second term, which can be rewritten as

$$S_{\rm TPC}(\Gamma) = -\frac{i}{\hbar}\int dt \int dt' \int_{-\infty}^{\infty} d\tau\; e^{i\omega(t-t')}\mathrm{tr}\Big\{E_2^\dagger(\omega_r)E_2(\omega_r)\mathcal{T}[E_1^\dagger(t)E_1(t'), H_{\rm int}(\tau)]\varrho(\tau)\Big\}. \tag{A3}$$

The commutator may be evaluated to

$$\begin{aligned}&[E_1^\dagger(t)E_1(t'), H_{\rm int}(\tau)]\\ =&E_1^\dagger(t)[E_1(t'), E_1^\dagger(\tau)V(\tau)] + [E_1^\dagger(t), E_1(\tau)V^\dagger(\tau)]E_1(t') \quad \text{(A4)}\\ =&E_1^\dagger(t)V(\tau)\delta(t'-\tau) - V^\dagger(\tau)\delta(t-\tau)E_1(t'), \quad \text{(A5)}\end{aligned}$$

which allows us to write the final signal as

$$\begin{aligned}S_{\rm TPC}(\Gamma) = -\frac{i}{\hbar}\int dt \int e^{i\omega(t-t')}\\ \times \mathrm{tr}\Big\{E_2^\dagger(\omega_r)E_2(\omega_r)\Big(E_1^\dagger(t)V(t')\varrho(t') - E_1(t')V^\dagger(t)\varrho(t)\Big)\Big\},\end{aligned} \tag{A6}$$

and the two terms can be combined to Eq. (5).

Appendix B: The entangled-photon correlation function

This appendix summarizes the light field created by parametric downconversion. We start with the form [7]

$$\varrho_{\rm field} = U_{\rm PDC}|0\rangle\langle 0|U_{\rm PDC}^\dagger, \tag{B1}$$

where the transformation U is created by the effective downconversion Hamiltonian

$$U_{\rm PDC} = \exp\Big[-\frac{i}{\hbar}H_{\rm PDC}\Big], \tag{B2}$$

$$\text{with} \qquad H_{\rm PDC} = \int d\omega_a \int d\omega_b\; \Phi(\omega_a,\omega_b)a_1^\dagger(\omega_a)a_2^\dagger(\omega_b) - h.c. \tag{B3}$$

We only work in the weak downconversion limit, in which we can approximate the exponential by

$$U_{\rm PDC} \approx \mathcal{I} - \frac{i}{\hbar}H_{\rm PDC} + \cdots. \tag{B4}$$

In this situation, the four-point field correlation functions we need to evaluate take a particularly simple form

$$\begin{aligned}&\langle E_1^\dagger(\omega_r)E_2^\dagger(\omega)E_2(\omega_b)E_1(\omega_r)\rangle\\ =&\Big(-\frac{i}{\hbar}\Big)^4\Phi^*(\omega_r,\omega)\Phi(\omega_r,\omega_b).\end{aligned} \tag{B5}$$

1. The two-photon amplitude

The so-called two-photon amplitude is given by

$$\Phi(\omega_a,\omega_b) = \alpha A_p(\omega_a+\omega_b)\;\exp\Big[-\gamma(\Delta k(\omega_a,\omega_b)L)^2\Big], \tag{B6}$$

where A_p denotes the normalized envelope of the pump pulse, which we chose to be a Gaussian around the central pump frequency ω_p, *i.e.*

$$A_p(\omega) = \frac{1}{\sqrt{2\pi}\sigma_p}e^{-(\omega-\omega_p)^2/(2\sigma_p^2)}. \tag{B7}$$

α is a constant containing the second-oder susceptibility of the crystal, the quantization area of the fields, the dielectric constant, as well as the crystal length. The second term

$\exp[-\gamma(\Delta kL)^2]$ is the so-called phase-matching function with $\Delta k(\omega_a, \omega_b) = k_p(\omega_a+\omega_b)-k_1(\omega_a)-k_2(\omega_b)$ the phase mismatch between the wavevectors of the involved field. $\gamma = 0.04822$ is a numerical constant to fit the spectrum to observed bandwidths [7]. In type-II downconversion, the phase mismatch may be approximated linearly around the central frequencies of the two beams,

$$\Delta k(\omega_a, \omega_b) = \left(\omega_a - \omega_p/2\right) T_1 + \left(\omega_b - \omega_p/2\right) T_2. \quad \text{(B8)}$$

The two timescales T_1 and T_2 are determined by the differences between the group velocities of the downconverted photons in beams 1 and 2, and the one of the pump pulse times the length of the crystal [6]. We consider the following parameters,

$$T_1 = -0.00007(T/fs) \text{ cm}, \quad \text{(B9)}$$
$$T_2 = 0.00025(T/fs) \text{ cm}, \quad \text{(B10)}$$

which have been parametrized with respect to the so-called entanglement time $T = T_2 - T_1$ (in fs) [24]. We finally note that in contrast to most applications of these entangled photons, our simulations work in the regime of positive frequency correlations [19]. Here, the bandwidth of the pump pulse is much larger than the inverse entanglement time, $\sigma_p \ll 1/T$.

[1] M. Kira, S. W. Koch, R. Smith, A. E. Hunter, and S. Cundiff, Nature Phys. **7**, 799 (2011).
[2] J. Javanainen and P. L. Gould, Phys. Rev. A **41**, 5088 (1990).
[3] B. Dayan, A. Pe'er, A. A. Friesem, and Y. Silberberg, Phys. Rev. Lett. **94**, 043602 (2005).
[4] D.-I. Lee and T. Goodson, J. Phys. Chem. B **110**, 25582 (2006), http://pubs.acs.org/doi/pdf/10.1021/jp066767g.
[5] Y. Shih, Reports on Progress in Physics **66**, 1009 (2003).
[6] W. P. Grice and I. A. Walmsley, Phys. Rev. A **56**, 1627 (1997).
[7] A. Christ, K. Laiho, A. Eckstein, K. N. Cassemiro, and C. Silberhorn, New Journal of Physics **13**, 033027 (2011).
[8] O. Roslyak and S. Mukamel, Phys. Rev. A **79**, 063409 (2009).
[9] F. Schlawin, K. E. Dorfman, B. P. Fingerhut, and S. Mukamel, Nature Communications **4**, 1782 (2013).
[10] M. G. Raymer, A. H. Marcus, J. R. Widom, and D. L. P. Vitullo, The Journal of Physical Chemistry B **117**, 15559 (2013).
[11] H. Oka, The Journal of Chemical Physics **134**, 124313 (2011).
[12] H. Oka, The Journal of Chemical Physics **135**, 164304 (2011).
[13] A. Yabushita and T. Kobayashi, Phys. Rev. A **69**, 013806 (2004).
[14] A. Kalachev, D. Kalashnikov, A. Kalinkin, T. Mitrofanova, A. Shkalikov, and V. Samartsev, Laser Physics Letters **4**, 722 (2007).
[15] A. Kalachev, D. Kalashnikov, A. Kalinkin, T. Mitrofanova, A. Shkalikov, and V. Samartsev, Laser Physics Letters **5**, 600 (2008).
[16] D. A. Kalashnikov, Z. Pan, A. I. Kuznetsov, and L. A. Krivitsky, Phys. Rev. X **4**, 011049 (2014).
[17] K. E. Dorfman, F. Schlawin, and S. Mukamel, The Journal of Physical Chemistry Letters **5**, 2843 (2014).
[18] P. J. Mosley, J. S. Lundeen, B. J. Smith, P. Wasylczyk, A. B. U'Ren, C. Silberhorn, and I. A. Walmsley, Phys. Rev. Lett. **100**, 133601 (2008).
[19] Y.-W. Cho, K.-K. Park, J.-C. Lee, and Y.-H. Kim, Phys. Rev. Lett. **113**, 063602 (2014).
[20] S. Mukamel and S. Rahav, in *Advances in Atomic, Molecular, and Optical Physics*, Advances In Atomic, Molecular, and Optical Physics, Vol. 59, edited by P. B. E. Arimondo and C. Lin (Academic Press, 2010) pp. 223 – 263.
[21] Y. Tanimura, Journal of the Physical Society of Japan **75**, 082001 (2006).
[22] F. Šandra and S. Mukamel, The Journal of Chemical Physics **125**, 014507 (2006).
[23] K. E. Dorfman, B. P. Fingerhut, and S. Mukamel, The Journal of Chemical Physics **139**, 124113 (2013).
[24] B. E. A. Saleh, B. M. Jost, H.-B. Fei, and M. C. Teich, Phys. Rev. Lett. **80**, 3483 (1998).